VOL 3, NO.1 (2023) 48-72
https://jagst.utm.my

JAGST
Journal of Advanced Geospatial Science & Technology

Boosting Ensemble Learning Technique for Landslide Activity Classification using Vegetation Anomalies Indicators

Mohd Radhie Mohd Salleh[1*], Muhammad Zulkarnain Abdul Rahman[1], Zamri Ismail[2], Mohd Faisal Abdul Khanan[2], Mohamad Jahidi Osman[1], Mohd Asraff Asmadi[1], and Suhaini Mohamad Sukairi[3]
[1]TropicalMap Research Group, Faculty of Built Environment and Surveying, Universiti Teknologi Malaysia, 81310 Johor Bahru, Johor, Malaysia
[2]Geospatial Imaging and Information Research Group (GI2RG), Faculty of Built Environment and Surveying, Universiti Teknologi Malaysia, 81310 Johor Bahru, Johor, Malaysia
[3]Faculty of Civil Engineering, Universiti Teknologi Malaysia, 81310 Johor Bahru, Johor, Malaysia
*Email: mohdradhie.gis@gmail.com

Abstract – Having detailed information and inventories about landslides is important for studying landslides. These inventories have been created for various purposes. However, detecting and mapping landslides in highly dense vegetated areas and evaluating their activity state is a major challenge due to various factors, such as the dense tree canopy, undulating terrain, and fast-growing vegetation. Therefore, this paper presents a new technique for categorising landslide activity using vegetation anomalies indicators (VAIs) extracted from high-resolution remote sensing data. The data were utilised to support manual landslide inventory and VAI production. The landslide inventory map was divided randomly into two groups of datasets, one for training (70%) and the other for validation (30%). The classification process used a boosting ensemble learning approach, specifically Decision Tree (DT) and Stochastic Gradient Boosting (SGB), with seven primary VAIs as inputs. The study compared the classification models' performance against various parameters, including spatial resolution and landslide depth. To evaluate the accuracy of the classification methods, metrics such as overall accuracy, kappa, producer's accuracy, and user's accuracy were measured from the validation dataset. The results demonstrated that both methods performed best under high spatial resolution. Among the two approaches, DT performed better, with an overall accuracy value of 89.6% for deep-seated translational, 64.0% for shallow translational, 67.0% for deep-seated rotational, and 80.0% for shallow rotational. This reliable accuracy that has been attained in landslide activity classification from VAI allows (i) to map and classify the landslide activity in the forested area, (ii) characterise the different types of vegetation characteristics to specific landslide activity, and (iii) permits for the continuous landslide activity monitoring in the area where monitoring activity is not practically feasible to be conducted.

Keywords *– Landslide, GIS, Remote Sensing, Machine Learning*

Article History: Received 18 February 2023, Accepted 28 March 2023, Published 31 March 2023

How to cite: Mohd Salleh, M. R., Abdul Rahman, M. Z., Ismail, Z., Abdul Khanan, M. F., Osman, M. J., Asmadi, M. A. and Mohamad Sukairi, S. (2023). Boosting Ensemble Learning Technique for Landslide Activity Classification using Vegetation Anomalies Indicator. Journal of Advanced Geospatial Science and Technology. 3(1), 48-72.

1. Introduction

Landslides severely threaten human life in various parts of the world (Schuster, 1996, GEOHAZARDS, 2004). They impact civilians, the environment, properties, and infrastructure (Gaidzik et al., 2017, Kaur et al., 2017, Mia et al., 2015, Schuster and Highland, 2003). Landslides are defined as mass movements on natural or man-made slopes involving the shifting of slope-forming materials such as soil and rock by falling, toppling, sliding, spreading, or flowing (Cruden, 1991, Gariano and Guzzetti, 2016). The Centre for Research on the Epidemiology of Disasters (CRED) database recorded over 9,000 landslide-related deaths from 2006 to 2015, with Asia accounting for 77.4% of fatalities (Sanderson & Sharma, 2016).

Having comprehensive records of landslides and associated information is vital for landslide research. The creation of landslide inventory maps serves several purposes (Brabb, 1991), such as (i) documenting landslide activity in various areas, from small to a large area (Cardinali et al., 2001), (ii) documenting landslide occurrences at regional, state, and national levels (Brabb and Pampeyan, 1972, Cardinali et al., 1990, Duman et al., 2005), and as a precursor to producing landslide susceptibility, hazard, and risk assessments (Dias et al., 2021, Hung et al., 2017, Van Westen et al., 2006). Furthermore, inventory maps aid in analysing landslide distribution, types, and patterns related to drainage, morphological, and vegetation characteristics (Guzzetti et al., 1996, Soeters and Westen, 1996). In the past, landslide inventory mapping involved fieldwork in which an interpreter could recognise landslide types and activity based on various diagnostic features. However, this approach is not always economically or practically feasible, particularly at the regional scale, where time-consuming and resource-intensive procedures are required (Getachew and Meten, 2021, Kocaman et al., 2020, Pawłuszek et al., 2017, Yang et al. 2017, Behling et al., 2014, Cigna et al., 2013, Santangelo et al., 2010, Haneberg et al., 2009, Guzzetti et al., 1999). Additionally, old landslides, total or partial vegetation coverage, and features dismantled by other landslides or human actions can make it challenging to observe all of a landslide (Guzzetti et al., 2012).

Using remote sensing data alongside conventional investigations can effectively support landslide mapping due to its comprehensive area coverage, non-invasive nature, and cost-effectiveness (Moosavi et al., 2014, Golovko et al., 2015, Bozzano et al., 2017). Aerial photographs are commonly used to recognise landslides and cover a wide area (Otukei and Blaschke, 2010, Guzzetti et al., 2012, Chen et al., 2013, Li et al., 2016). However, this technique requires

experience, training, and a well-defined landslide interpretation standard (Antonini et al., 2002, Galli et al., 2008, Jackson Jr et al., 2012). Furthermore, it may produce errors, particularly in forest areas where vegetation can conceal underlying soils and rocks (Marchesini et al., 2013, Santangelo et al., 2015), especially for forest areas (Brardinoni et al., 2003, Mezaal et al., 2017, Pirasteh and Li, 2016), since the reflectance spectra of vegetation conceal the spectra of underlying soils and rocks, the most critical barrier to geological identification and mapping (McKean and Roering, 2004, Hede et al., 2015). In addition, using monoscopic and stereoscopic images from aerial photographs might produce a digital terrain model (DTM) with low accuracy since the ground surface is not well presented in photogrammetric DTMs of forested terrain, leading to incomplete and unreliable landslide inventories. For this reason, using vegetation information to indicate landslide activity is a natural and inexpensive approach, especially in tropical regions where vegetation can stabilise slopes through root binding.

The stability of a slope may be improved by vegetation, as plant roots bind the soil and reinforce its layers. Researchers have used various Vegetation Anomalies Indices (VAIs), such as tree height irregularities (Razak et al., 2013a, Razak et al., 2013b), leaning trunks (Wang et al., 2016a, Wang et al., 2016b, Zhang et al., 2016), and tree-rings (Łuszczyńska et al., 2017, Wistuba et al., 2013), to investigate the relationship between vegetation characteristics and landslide occurrences. However, there has been limited research in tropical regions. This is because many tropical areas are inaccessible or difficult to reach, making it challenging to collect data on landslide activity and vegetation indicators (Yan et al., 2023). Also, the factors include a lack of transportation infrastructure or restricted access to protected areas. Besides that, vegetation patterns in tropical regions can be highly variable and complex, which can make it difficult to identify clear indicators of landslide activity (Brardinoni et al., 2003, McKean and Roering, 2004, Korup, 2005, Cigna et al., 2013, Tien Bui et al., 2018). This variability can be due to soil type, topography, and climate. Therefore, this study uses high-resolution, remotely sensed data, such as satellite images and airborne LiDAR, to derive various VAIs and examine their relationship with landslide activity. The goal is to explore the possibility of using VAIs to automatically detect landslides, which could help guide in-situ landslide activity monitoring and reduce the need for labour-intensive manual image interpretation in large landslide zones in tropical areas.

2. Study Area

Kundasang is a region in the northwest of Ranau, Sabah, Malaysia, with a hilly and unstable landscape caused by historical tectonic activity (Figure 1). The study area encompasses 70.47 km2 and ranges from 500 to 2000 meters above sea level. The climate is tropical and humid, with temperatures between 25 °C and 35 °C in lowlands and two monsoon seasons from May to October (dry) and November to April (wet). Kundasang is in the "ever-wet zone" and receives at least 60 mm of rainfall per month, with an annual rainfall average of 2075 mm (ranging from 1920 mm to 3190 mm). This location was chosen for the study due to its tropical setting and high incidence of landslides from natural and human causes (Tating, 2006).

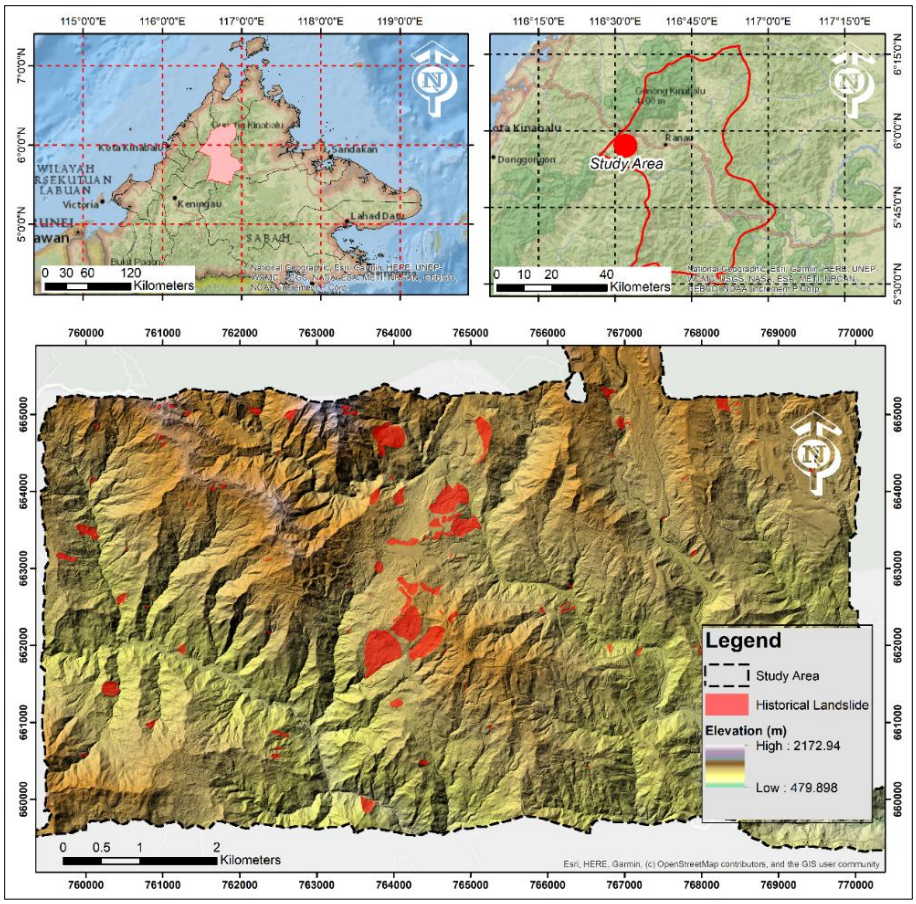

Figure 1. Location of the study area

3. Materials and Methods

The study is divided into multiple phases. The initial stage involves obtaining high-resolution remotely sensed data, field data, and ancillary data. The point cloud data (Figure 2) originated from a RIEGL LMS-Q680i airborne laser scanner in 2015, a laser scanner that can detect over long distances and analyse full waveforms as acquired from the Department of Mineral and Geosciences Malaysia (JMG). This scanner can acquire scan data with a precision of 20mm and has a range of 3000m, allowing for measurement of up to 266,000 pulses per second on the ground. As a result, the point cloud data is of very high density, with an average of 160 points per square meter (m^2) in the study area. To differentiate between ground and non-ground points, the airborne LiDAR data was processed using the Triangular Irregular Network (TIN) densification method suggested by Axelsson (1999). Airborne LiDAR point clouds are filtered and interpolated to create a Digital Terrain Model (DTM), while a Digital Surface Model (DSM) is produced by interpolating non-ground points. Field data is also collected during this stage, which includes observing landslide inventory and vegetation characteristics.

The second stage focuses on developing a landslide inventory by manually interpreting the high-resolution, remotely sensed data. The landslide inventory was created through remote sensing data interpretation and field observations. The remote sensing component of the inventory relied on several airborne LiDAR-derived datasets: topographic openness, hillshade, and colour composite. These datasets were created using a DTM and orthophoto with a spatial resolution of 7 cm. Topographic openness was used to identify the contrast between the flat and downward slopes and was detected by examining a colour ramp. Other landslide features, such as hummocky surfaces, steep slopes, thick toes, and step-like morphologies, could be recognised using the hillshade 3D features. The orthophoto image displayed evidence of landslide occurrence through polygons or other indicators such as road cracks, soil erosion, and ponding or back-tilting areas.

The third stage concentrates on developing VAIs using high-resolution remote sensing data. The VAIs consisted of 15 raster maps that can be grouped into seven groups: 1) tree height irregularities; 2) canopy gap; 3) density of different layers of vegetation; 4) vegetation type; 5) vegetation indices; 6) root strength index (RSI); and 7) distribution of water-loving trees. During the fifth stage, VAI maps and landslide inventory maps were combined and analysed to classify landslide activity. A boosting ensemble learning approach was used, as shown in the following pseudocode (see Table 1), to classify different types and depths of landslides, such as deep-seated

translation, shallow translational, deep-seated rotational, and shallow rotational. The Boosting technique was introduced as an online learning algorithm called Adaboost in 1997 by Freund and Schapire (1997). It involves creating a model from the training data and then developing a second model that aims to correct the errors of the first model. This process is repeated until the training data is perfectly predicted or until a maximum number of models is reached. The method constructs a linear combination of base learners focusing on challenging examples. Boosting has demonstrated significant success in supervised learning, and a weighted voting approach is utilised to generate the final strong learner.

The pseudocode for the Boosting algorithm is presented in Table 1. The Boosting algorithm requires three inputs: the training dataset *D*, a base learning algorithm *L*, and the number of learning rounds, *T*. The algorithm starts by initialising the weight distribution D_1. Then, for each round t = 1 to *T*, the algorithm trains a base learner h_T using a weighted version of the training data D_T. The error of the base learner is calculated as ε_t, and the weight of the base learner is determined as α_t. The normalisation factor Z_t is then computed to make the distribution D_{t+1}. Finally, the distribution for the next round, $D_{t+1}(i)$, is updated based on the weights and errors of the current base learner. This process is repeated for *T* rounds. This Boosting algorithm outputs a weighted combination of the *T* base learners, where the weight of each base learner is given by α_t. The final prediction is made by taking the sign of the sum of the weighted predictions.

The resulting classified landslide activity map was then assessed using the validation dataset from the landslide inventory. Various accuracy statistics, such as overall accuracy (OA), kappa coefficient (κ), producer's accuracy (PA), and user's accuracy (UA), were constructed using an error matrix (Foody, 2020, Maxwell et al., 2021). OA indicates the percentage of samples that were correctly classified. κ is a powerful and commonly used multivariate accuracy assessment technique that evaluates the overall statistical agreement of a confusion matrix, thereby assessing classification accuracy more rigorously. PA measures the inaccuracy that arises due to an omission (omission error) and shows the likelihood of an actual class being correctly categorised. Conversely, UA is a measure of commission error that indicates the probability of a segment classified as predicted data representing the specific activity.

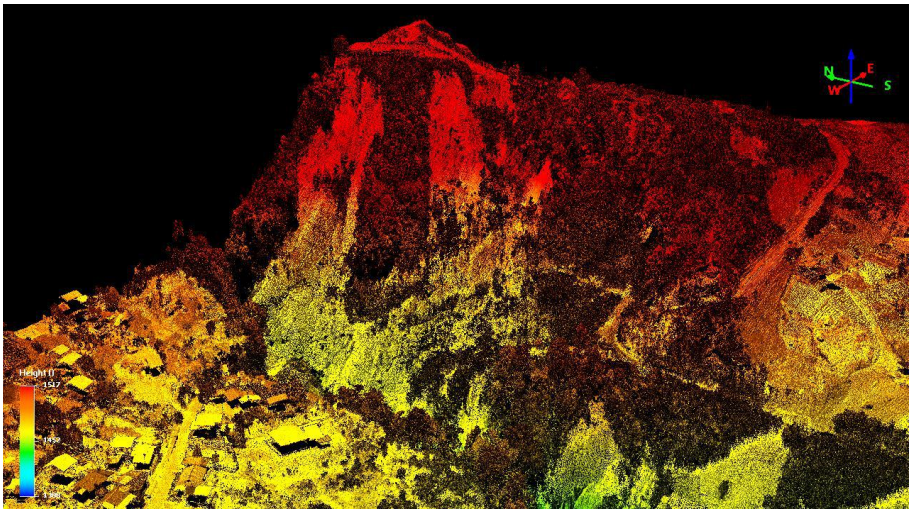

Figure 2. Visualisation of airborne LiDAR point cloud over part of the study area

Table 1. Pseudocode of boosting algorithm

Algorithm: Boosting

Input:

Dataset $D = [(x_1,y_1),(x_2,y_2),\ldots,(x_M,y_M)]$;

Base learning algorithm L;

Number of learning rounds, T.

Process:

$D_1(i) = \frac{1}{M}$; # Initialise the weight distribution

For $t = 1,2,\ldots,T$:

$h_T = L(D,D_T)$; #Train a base learner h_t from D using D_t

$\varepsilon_t = \sum_{i=1}^{M} D_t(i)[h_t(x_i) \neq y_1]$; #Measure the error of h_t

$\alpha_t = \frac{1}{2}\ln\frac{1-\varepsilon_t}{\varepsilon_t}$; #Determine the weight of h_t

$Z_t = \sum_{i=1}^{m} D_t(i) x \begin{cases} e^{-\alpha_t} \; if \; h_t(x_i) = y_i \\ e^{\alpha_t} \; if \; h_t(x_i) \neq y_i \end{cases}$; #Z_t is a normalisation factor that enables D_{t+1} to be a distribution

$D_{t+1}(i) = \frac{D_t(i)}{Z_t} x \begin{cases} e^{-\alpha_t} \; if \; h_t(x_i) = y_i \\ e^{\alpha_t} \; if \; h_t(x_i) \neq y_i \end{cases}$; #Update the distribution

end

Output:

$H(x) = sign \sum_{t-1}^{T} a_t h_t(x)$

4. Results and Discussion

The performance of landslide activity classification for deep-seated translational, shallow translational, deep-seated rotational, and shallow rotational landslides using boosting technique is presented in Figure 3 and Tables 2–5. The classification using boosting techniques (DT and SGB) achieved satisfactory accuracy for deep-seated translational landslides. The OA varied from 65.9%

to 89.6% and 65.9% to 81.8% for DT and SGB, respectively. Meanwhile, κ values ranged from 0.449–0.830 for the DT technique and 0.412–0.698 for SGB. Table 2 shows that DT consistently reported the best OA for almost all spatial resolution categories except 5 m. with 89.6%, 84.2%, 80.8%, 78.3%, and 63.9% for 0.5 m, 1 m, 5 m, 10 m, and 20 m resolution categories, respectively. Moreover, κ value also shows that DT has achieved a significant increase in classification accuracy with recorded κ values of 0.830 (0.5 m), 0.742 (1 m), 0.688 (5 m), 0.647 (10 m), and 0.449 (20 m). The increase of 23.7% of OA from 65.9% (20 m) to 89.6% (0.5 m) for DT and 15.9% for SGB indicated that the higher the spatial resolution, the more stable the OA result.

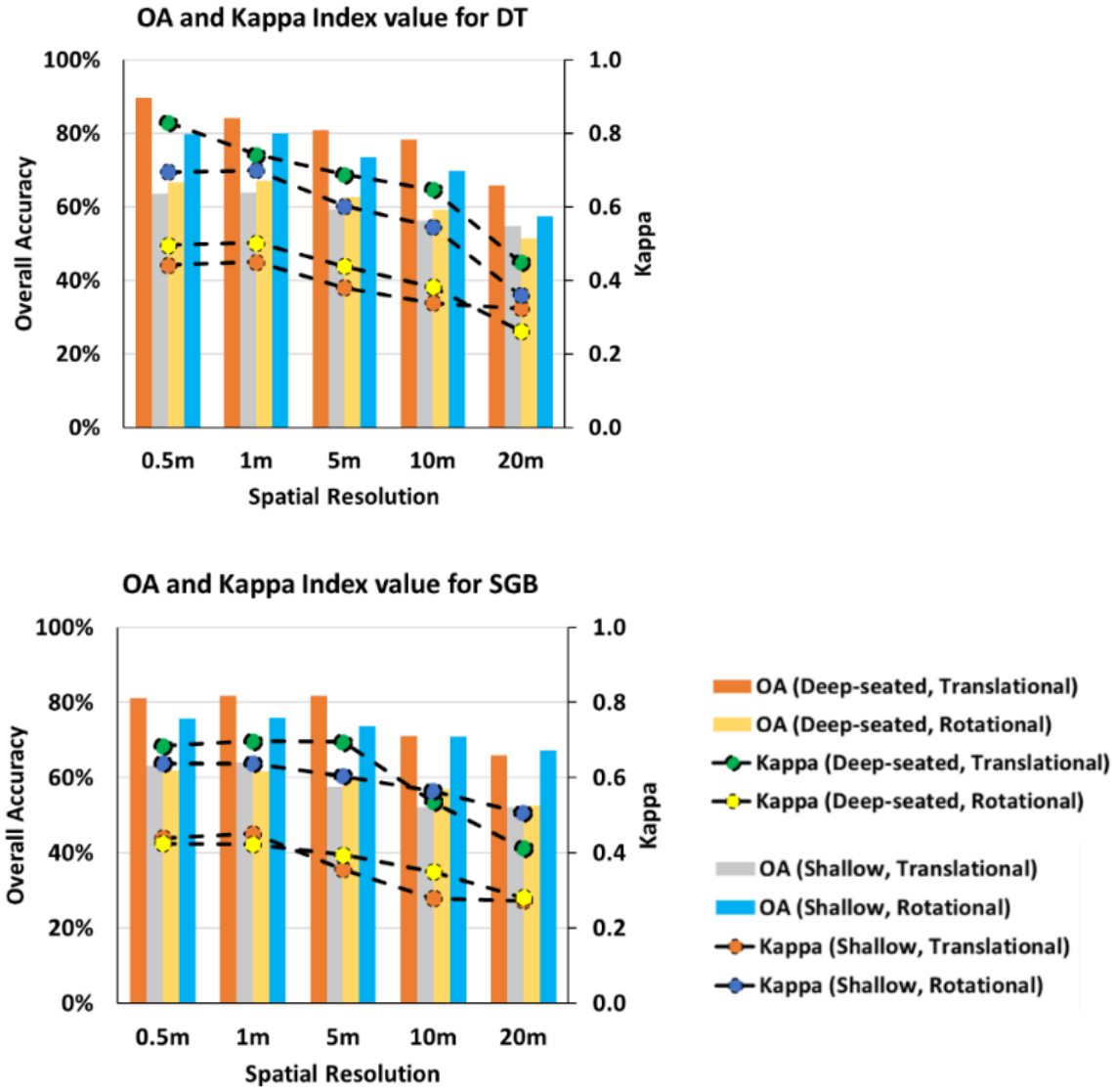

Figure 3. Graphs of OA and κ using the DT and SGB methods

Table 2. Accuracy assessment of classified activities of deep-seated translational landslide using the boosting technique

Deep-seated, Translational							
Resolution	**Assessment**	**DT**			**SGB**		
		Active	**Dormant**	**Relict**	**Active**	**Dormant**	**Relict**
0.5-meter	**PA (%)**	82.4	90.3	99.2	69.8	87.1	82.5
	UA (%)	84.0	89.8	97.7	81.8	79.0	87.3
	OA (%)	89.6			81.2		
	κ	0.830			0.684		
1-meter	**PA (%)**	86.0	83.1	84.4	78.7	84.9	77.9
	UA (%)	83.3	87.1	78.1	83.0	81.5	81.0
	OA (%)	84.2			81.8		
	κ	0.742			0.698		
5-meter	**PA (%)**	82.0	79.8	81.9	74.4	87.1	78.3
	UA (%)	78.3	83.5	77.9	85.8	80.0	81.8
	OA (%)	80.8			81.8		
	κ	0.688			0.695		
10-meter	**PA (%)**	62.3	86.3	84.9	69.8	72.5	69.7
	UA (%)	91.7	73.4	77.8	72.6	69.9	71.9
	OA (%)	78.3			71.1		
	κ	0.647			0.536		
20-meter	**PA (%)**	63.6	62.5	77.8	36.4	75.0	77.8
	UA (%)	50.0	71.4	77.8	66.7	66.7	63.6
	OA (%)	65.9			65.9		
	κ	0.449			0.412		

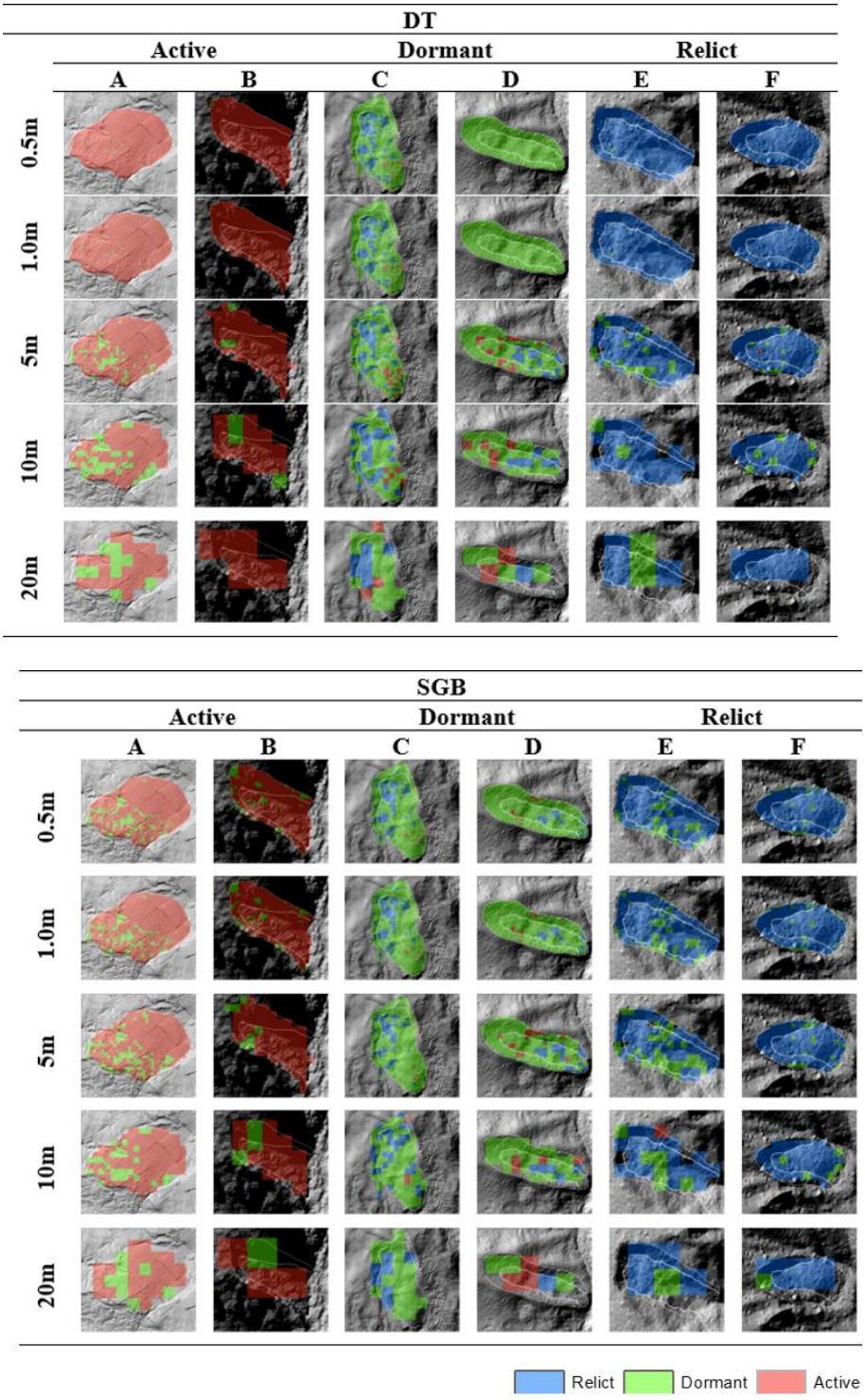

Figure 4. Examples of the classified activities of deep-seated translational landslides with different spatial resolutions using the DT and SGB methods

As shown in Table 3, in the case of shallow translational landslides, the classification of activity using boosting techniques is typically lower than in deep-seated translational landslides. The OA ranged from 54.8% to 64.0% and 52.1% to 63.9% for DT and SGB, respectively. Meanwhile, κ values ranged from 0.324 to 0.450 for the DT technique and 0.273 to 0.451 for SGB. Similar to the deep-seated translational, DT consistently reported the best OA for almost all spatial resolution categories with 63.4%, 64.0%, 59.3%, 56.2%, and 54.8% for 0.5 m, 1 m, 5 m, 10 m, and 20 m resolution categories, respectively. Moreover, the κ value also shows that DT has achieved a good classification accuracy with values of 0.442 (0.5 m), 0.450 (1 m), 0.380 (5 m), 0.338 (10 m), and 0.324 (20 m). The increase of 9.2% of OA from 54.8% (20 m) to 64.0% (1 m) for DT and 11.8% for SGB indicates that the higher the spatial resolution, the more stable the OA result. Both methods recorded the lowest OA values under the 20 m dataset spatial resolution category (DT = 54.8%, SGB = 52.1%). This is because the coarse resolution of the dataset tends to generalise the pixel value in the landslide location.

Table 3. Accuracy assessment of classified activities of shallow translational landslide using the boosting technique

Shallow, Translational							
Resolution	**Assessment**	**DT**			**SGB**		
		Active	**Dormant**	**Relict**	**Active**	**Dormant**	**Relict**
0.5-meter	**PA (%)**	48.1	68.2	70.4.	51.5	65.8	69.5
	UA (%)	67.3	60.6	64.4	64.0	61.9	64.1
	OA (%)	63.4			63.2		
	κ	0.442			0.440		
1-meter	**PA (%)**	47.8	68.9	71.5	52.1	65.5	71.4
	UA (%)	68.3	61.8	64.3	64.3	63.1	64.5
	OA (%)	64.0			63.9		
	κ	0.450			0.451		
5-meter	**PA (%)**	44.3	63.9	66.5	44.3	59.7	65.8
	UA (%)	64.4	54.8	61.3	55.9	54.7	61.4
	OA (%)	59.3			57.6		
	κ	0.380			0.356		
10-meter	**PA (%)**	44.4	60.6	62.4	42.0	49.5	64.7
	UA (%)	56.3	55.6	57.0	52.3	52.7	51.4
	OA (%)	56.2			52.1		
	κ	0.338			0.279		
20-meter	**PA (%)**	61.9	37.0	68.0	38.1	51.9	64.0
	UA (%)	50.0	43.5	70.8	50.0	50.0	55.2
	OA (%)	54.8			52.1		
	κ	0.324			0.273		

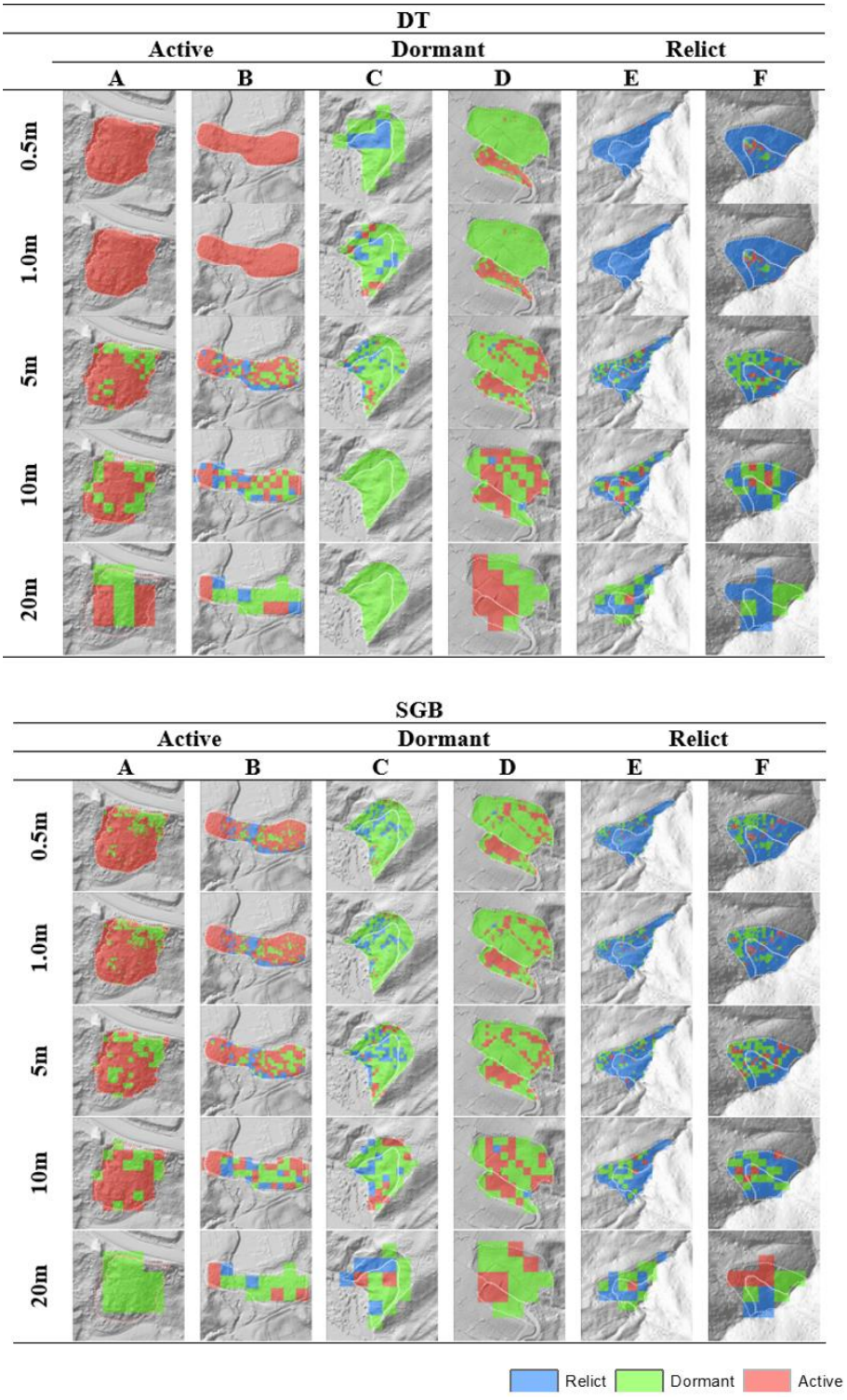

Figure 5. Examples of the classified activities of shallow translational landslides with different spatial resolutions using the DT and SGB methods

For deep-seated rotational landslides, the classification using all the methods achieved moderate accuracy results, where the OA was between 51.4% to 67.0% and 52.6% to 61.9% for DT and SGB, respectively, while the κ values ranged from 0.263 to 0.502 (DT) and 0.281 to 0.425 (SGB). Again, DT consistently yielded the highest OA for all spatial resolution categories except 20 m, with 66.6%, 67.0%, 62.8%, 59.1%, and 51.4% for 0.5 m, 1 m, 5 m, 10 m, and 20 m resolution categories, respectively. Moreover, the κ value also shows that DT has achieved a significant increase in classification accuracy with recorded values of 0.496 (0.5 m), 0.502 (1 m), 0.439 (5 m), 0.382 (10 m), and 0.263 (20 m). The increase of 15.6% of OA from 51.4% (20 m) to 67.0% (1 m) for DT and 9.3% for SGB indicates that the higher the spatial resolution, the more stable the OA result.

Table 4. Accuracy assessment of classified activities of deep-seated rotational landslide using the boosting technique

Deep-Seated, Rotational							
Resolution	**Assessment**	**DT**			**SGB**		
		Active	**Dormant**	**Relict**	**Active**	**Dormant**	**Relict**
0.5-meter	**PA (%)**	59.4	68.3	71.2	52.1	63.6	68.6
	UA (%)	65.1	66.1	68.2	60.9	60.9	63.5
	OA (%)	66.6			61.9		
	κ	0.496			0.425		
1-meter	**PA (%)**	59.3	68.7	71.9	51.8	63.4	68.9
	UA (%)	65.5	66.8	68.4	60.6	61.1	63.3
	OA (%)	67.0			61.8		
	κ	0.502			0.423		
5-meter	**PA (%)**	56.3	63.5	67.5	49.5	60.5	68.2
	UA (%)	59.9	63.4	64.4	57.7	59.6	61.7
	OA (%)	62.8			59.9		
	κ	0.439			0.395		
10-meter	**PA (%)**	46.4	64.2	65.0	43.1	61.1	64.7
	UA (%)	59.8	56.3	61.8	53.3	54.0	61.0
	OA (%)	59.1			56.9		
	κ	0.382			0.350		
20-meter	**PA (%)**	41.9	57.3	53.0	43.2	61.5	50.6
	UA (%)	48.4	52.4	52.4	50.0	55.7	50.6
	OA (%)	51.4			52.6		
	κ	0.263			0.281		

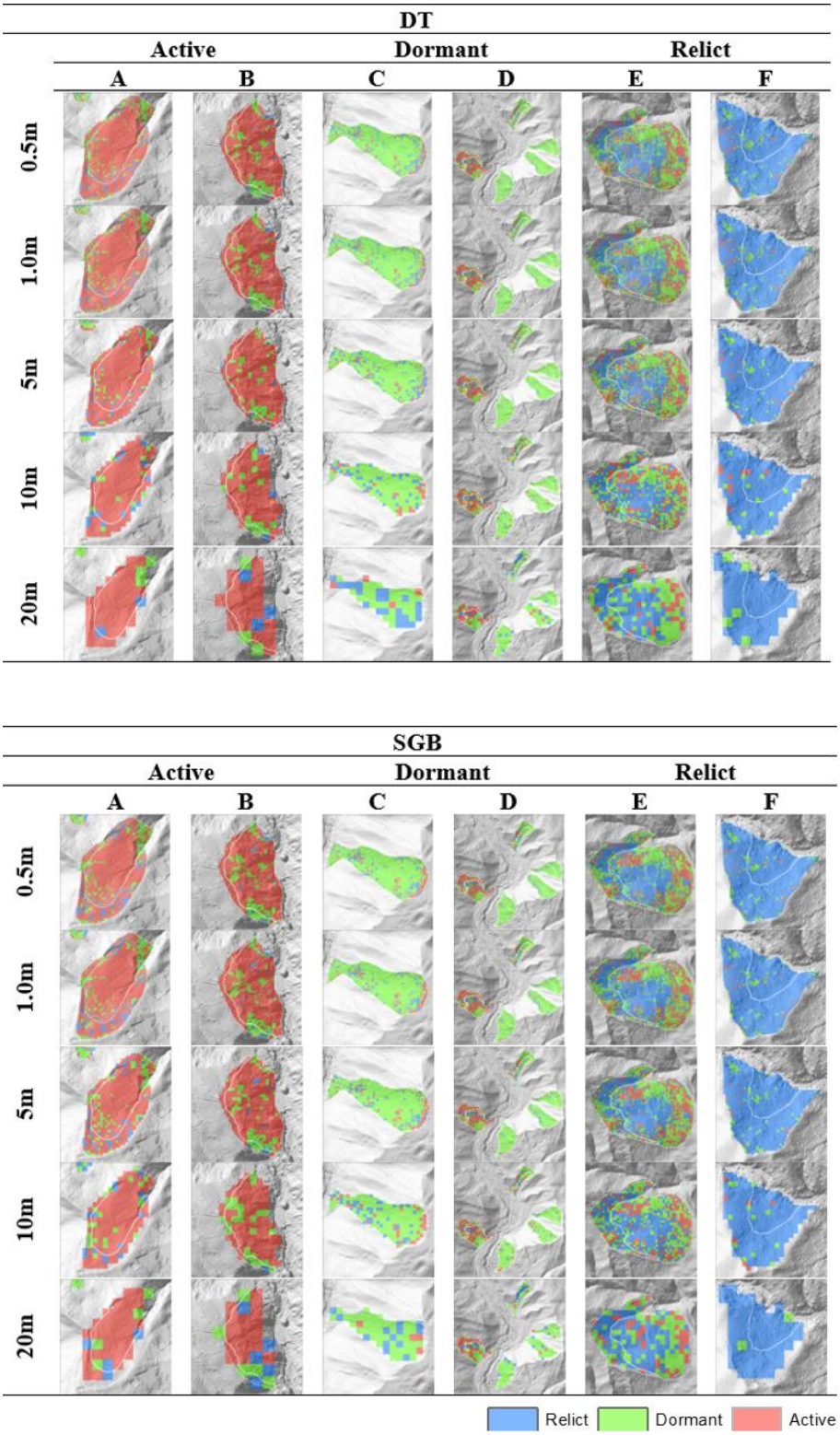

Figure 6. Examples of the classified activities of deep-seated rotational landslides with different spatial resolutions using the DT and SGB methods

The classification accuracy was satisfactory in shallow rotational landslides, as shown in Table 5. The OA was between 57.4% and 80.0% (DT) and 67.2% and 75.9% (SGB), while κ was between 0.360 and 0.669 (DT) and 0.506 and 0.638 (SGB). DT consistently reported the best OA especially high spatial resolution categories (0.5 m–5 m) with 79.7%, 80.0%, 73.6%, 69.7%, and 57.4% for 0.5 m, 1 m, 5 m, 10 m, and 20 m resolution categories, respectively. Additionally, the κ value shows that DT has achieved a significant increase in classification accuracy with values of 0.695 (0.5 m), 0.699 (1 m), 0.603 (5 m), 0.646 (10 m), and 0.360 (20 m). The OA for DT increased from 57.4% (20 m) to 80.0% (1 m) with changes of 22.6% and 8.7% for SGB, indicating that the OA remains steady when the spatial resolution size reduces.

Table 5. Accuracy assessment of classified activities of shallow rotational landslide using the boosting technique

Shallow, Rotational							
Resolution	**Assessment**	**DT**			**SGB**		
		Active	**Dormant**	**Relict**	**Active**	**Dormant**	**Relict**
0.5-meter	**PA (%)**	81.9	74.4	82.6	77.9	71.3	78.1
	UA (%)	84.0	81.1	73.9	81.6	74.7	70.8
	OA (%)	79.7			75.8		
	κ	0.695			0.637		
1-meter	**PA (%)**	82.3	74.1	83.4	78.1	70.6	78.7
	UA (%)	84.4	81.9	73.7	80.7	75.7	71.0
	OA (%)	80.0			75.9		
	κ	0.699			0.638		
5-meter	**PA (%)**	77.7	67.5	74.9	75.6	67.5	77.1
	UA (%)	76.3	72.0	72.0	77.4	71.1	71.8
	OA (%)	73.6			73.6		
	κ	0.603			0.603		
10-meter	**PA (%)**	74.4	60.9	75.0	75.6	58.6	80.9
	UA (%)	74.4	72.6	62.2	74.7	72.9	65.5
	OA (%)	69.7			71.0		
	κ	0.546			0.565		
20-meter	**PA (%)**	71.4	48.0	59.1	71.4	68.0	63.6
	UA (%)	50.0	57.1	65.0	50.0	70.8	82.4
	OA (%)	57.4			67.2		
	κ	0.360			0.506		

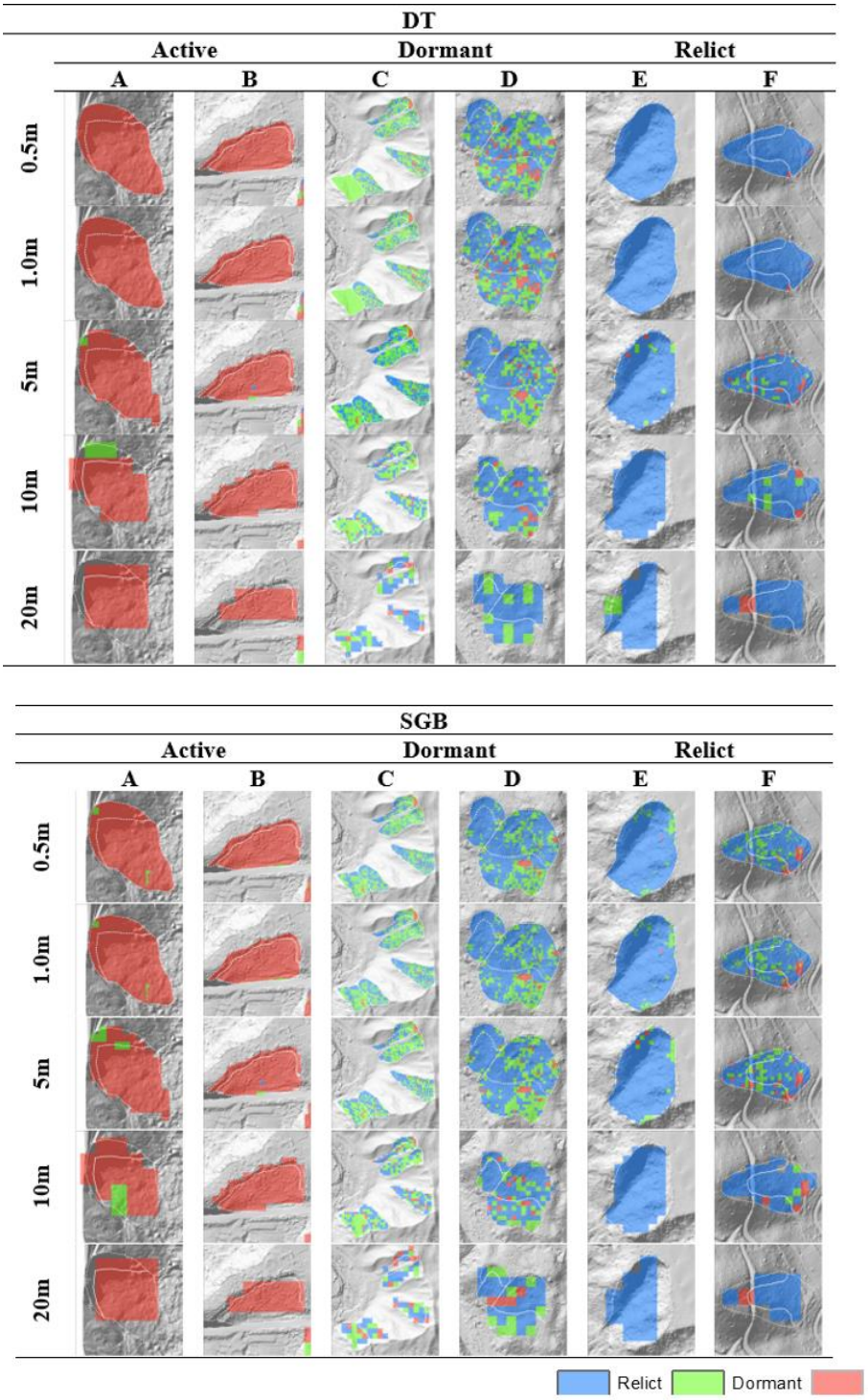

Figure 7. Examples of the classified activities of shallow rotational landslide with different spatial resolutions using the DT and SGB methods

The classification results for each activity class are analysed by measuring the producer's accuracy (PA) and the user's accuracy (UA). All the methods recorded reliable results of PA and UA for deep-seated translational landslides, especially for 0.5 m to 10 m spatial resolution categories, as stated in Table 2. The PA values ranged from 36.4%–86.0%, 62.5%–90.3%, and 69.7%–99.2% for active, dormant, and relict, respectively, while UA values ranged from 50.0%–91.7% (active), 66.7%–89.8% (dormant), and 63.6%–97.7% (relict). By averaging the PA and UA values for all the methods with specific spatial resolution categories, the active class recorded slightly higher UA than PA, with the highest average values of 83.1% and 82.4%, respectively. This indicates the lesser magnitude of misclassification of other categories as active classes (low commission errors). However, the misclassification of the active class, mainly dormant landslides, can be examined from the classified results as depicted in Figure 4, indicating that the active class also had omission errors, particularly for large spatial resolution size categories. Meanwhile, dormant and relict classes exhibited nearly the same PA and UA in the classified landslides, indicating the prevalence of significantly considerable spectral/variable homogeneity in them, with the highest average values of 88.7% (PA) and 84.4% (UA) for dormant, and 90.8% (PA) and 92.5% (UA) for relict. Both classes experienced low omission and commission errors in the classified results. In the case of shallow translational landslides, the PA values ranged from 38.1%–61.9%, 37.0%–68.9%, and 62.4%–71.5% for active, dormant, and relict classes, respectively. Meanwhile, UA values ranged from 50.0% to 68.3% for active, 43.5% to 63.1% for dormant, and 51.4% to 70.8% for relict. For the active class, the highest average values of UA (66.3%) and PA (50.0%) were classified as moderate and poor, respectively. This finding indicates that there were clear omissions of the active class (classified as dormant) in the results, as depicted in Figure 5. For the dormant class, moderate values of UA and PA were recorded, with the highest average values of 62.5% and 67.2%, respectively. The PA of relict was high (the highest average value of 71.5%), indicating that the relict class had low omissions and high commissions observed from the classified results since a moderate value of UA was recorded.

For deep-seated rotational landslides, the PA values ranged from 41.9%–59.4%, 57.3%–68.7%, and 50.6%–71.9% for active, dormant, and relict classes, respectively, while UA values ranged from 48.4%–65.5% (active), 52.4%–66.8% (dormant), and 50.6%–68.4% (relict), which can be categorised as moderate results. The active class exhibited much higher UA than PA in the classified landslide, with the highest average values of 55.7% (PA) and 63.1% (UA). Dormant class

results were substantially identical to active class results, with maximum averages of 66.0% and 64.0% for PA and UA, respectively, while the relict class recorded slightly higher values than the dormant class, with 70.4% (PA) and 65.9% (UA). The assessment of PA and UA showed satisfactory accuracy results for shallow rotational landslides, especially for 0.5 m to 10 m spatial resolution categories. The PA values ranged from 71.4%–82.3%, 48.0%–74.4%, and 59.1%–83.4% for active, dormant, and relict classes, respectively, while UA values ranged from 50.0%–84.4% (active), 57.1%–81.9% (dormant), and 62.2%–82.4% (relict). By averaging the PA and UA values, boosting technique yielded satisfactory results with 80.2% (PA) and 82.8% (UA) for the active class, 72.9% (PA) and 78.8% (UA) for the dormant class, and 81.1% (PA) and 72.3% (UA) for relict class. By visualising the classification results, as shown in Figure 7, the dormant class tends to be classified as a relict class (omission error), especially for large spatial resolution size categories—the misclassification of dormant as relict was obvious, due to both classes' sharing similar vegetation characteristics.

5. Conclusion

Landslide state of activity classification in tropical forests can be more challenging than in other regions due to the complex and dynamic nature of tropical forest ecosystems. The dense vegetation cover, varied topography, and high rainfall can make detecting signs of instability or movement on slopes difficult. Furthermore, landslide activity in tropical forests can be influenced by a range of factors, including the types of trees and other vegetation, soil characteristics, and the intensity and duration of rainfall. This means that a more detailed and comprehensive assessment of the area may be required to classify the state of landslide activity accurately. Vegetation can provide essential clues to the stability of a slope and can be used to help classify landslide states of activity in tropical forests. Therefore, this study has utilised VAIs as a predictor in classifying landslide activity. Two types of boosting techniques were used, namely DT and SGB.

In summary, boosting technique, i.e. DT and SGB, successfully classified the landslide activity using VAIs, whereas the DT method produced higher accuracy results than the SGB approach. The maximum OA of 89.6%, 64.0%, 61.9%, and 80.0% for deep-seated, shallow, deep-seated, and shallow rotational, respectively, indicates that different landslide types and depths could produce different accuracy results. Analysing the spatial resolution's effect on classification

accuracy, better accuracy results were obtained for high spatial resolution categories regardless of the different parameter setting algorithms used.

Acknowledgements

The authors would like to thank TropicalMap Research Group for supporting this study. Also, we appreciate the comments of the anonymous reviewers in revising the paper.

References

Antonini, G., Ardizzone, F., Cardinali, M., Galli, M., Guzzetti, F., & Reichenbach, P. (2002). Surface deposits and landslide inventory map of the area affected by the 1997 Umbria-Marche earthquakes. *Bollettino della Società Geologica Italiana, 121*(1), 843-853.

Axelsson, P. (1999). Processing of laser scanner data—algorithms and applications. *ISPRS Journal of Photogrammetry and Remote Sensing, 54*(2-3), 138-147.

Behling, R., Roessner, S., Kaufmann, H., & Kleinschmit, B. (2014). Automated spatiotemporal landslide mapping over large areas using rapid eye time series data. *Remote Sensing, 6*(9), 8026-8055.

Bozzano, F., Mazzanti, P., Perissin, D., Rocca, A., De Pari, P., & Discenza, M. E. (2017). Basin scale assessment of landslides geomorphological setting by advanced InSAR analysis. *Remote Sensing, 9*(3), 267.

Brabb, E. E. (1991). The world landslide problem. *Episodes Journal of International Geoscience, 14*(1), 52-61.

Brabb, E. E., & Pampeyan, E. H. (1972). *Preliminary map of landslide deposits in San Mateo County, California*.

Brardinoni, F., Slaymaker, O., & Hassan, M. A. (2003). Landslide inventory in a rugged forested watershed: A comparison between air-photo and field survey data. *Geomorphology, 54*(3-4), 179-196.

Cardinali, M., Antonini, G., Reichenbach, P., & Guzzetti, F. (2001). Photo-geological and landslide inventory map for the Upper Tiber River basin. *CNR, Gruppo Nazionale per la Difesa dalle Catastrofi Idrogeologiche, Publication* (2154).

Cardinali, M., Guzzetti, F., & Brabb, E. E. (1990). *Preliminary maps showing landslide deposits and related features in New Mexico* (2331-1258).

Chen, J. W., Chue, Y. S., & Chen, Y. R. (2013). The application of the genetic adaptive neural network in landslide disaster assessment. *Journal of Marine Science and Technology, 21*(4), 442-452.

Cigna, F., Bianchini, S., & Casagli, N. (2013). How to assess landslide activity and intensity with Persistent Scatterer Interferometry (PSI): the PSI-based matrix approach. *Landslides, 10*(3), 267-283.

Cruden, D. M. (1991). A simple definition of a landslide. *Bulletin of the International Association of Engineering Geology-Bulletin de l'Association Internationale de Géologie de l'Ingénieur, 43*(1), 27-29.

Dias, H. C., Hölbling, D., & Grohmann, C. H. (2021). Landslide susceptibility mapping in Brazil: a review. *Geosciences, 11*(10), 425.

Duman, T. Y., Can, T., Emre, Ö., Keçer, M., Doğan, A., Ateş, Ş., & Durmaz, S. (2005). Landslide inventory of northwestern Anatolia, Turkey. *Engineering Geology, 77*(1-2), 99-114.

Foody, G. M. (2020). Explaining the unsuitability of the kappa coefficient in the assessment and comparison of the accuracy of thematic maps obtained by image classification. *Remote Sensing of Environment, 239*, 111630.

Freund, Y., & Schapire, R. E. (1997). A decision-theoretic generalisation of online learning and an application to boosting. *Journal of Computer and System Sciences, 55*(1), 119-139.

Gaidzik, K., Ramírez-Herrera, M. T., Bunn, M., Leshchinsky, B. A., Olsen, M., & Regmi, N. R. (2017). Landslide manual and automated inventories, and susceptibility mapping using LIDAR in the forested mountains of Guerrero, Mexico. *Geomatics, Natural Hazards and Risk, 8*(2), 1054-1079.

Galli, M., Ardizzone, F., Cardinali, M., Guzzetti, F., & Reichenbach, P. (2008). Comparing landslide inventory maps. *Geomorphology, 94*(3-4), 268-289.

Gariano, S. L., & Guzzetti, F. (2016). Landslides in a changing climate. *Earth-Science Reviews, 162*, 227-252.

GEOHAZARDS, I. (2004). GEOHAZARDS theme report: For the Monitoring of our Environment from Space and from Earth. *European Space Agency Publication*.

Getachew, N., & Meten, M. (2021). Weights of evidence modeling for landslide susceptibility mapping of Kabi-Gebro locality, Gundomeskel area, Central Ethiopia. *Geoenvironmental Disasters, 8*(1), 6. doi:10.1186/s40677-021-00177-z

Golovko, D., Roessner, S., Behling, R., Wetzel, H. U., & Kleinschmidt, B. (2015). Development of multi-temporal landslide inventory information system for southern Kyrgyzstan using GIS and satellite remote sensing. *Photogrammetrie-Fernerkundung-Geoinformation (PFG), 2015*(2), 157-172.

Guzzetti, F., Cardinali, M., & Reichenbach, P. (1996). The Influence of Structural Setting and Lithology on Landslide Type and Pattern. *Environmental and Engineering Geoscience, II*(4), 531-555. doi:10.2113/gseegeosci.II.4.531

Guzzetti, F., Carrara, A., Cardinali, M., & Reichenbach, P. (1999). Landslide hazard evaluation: a review of current techniques and their application in a multi-scale study, Central Italy. *Geomorphology, 31*(1-4), 181-216.

Guzzetti, F., Mondini, A. C., Cardinali, M., Fiorucci, F., Santangelo, M., & Chang, K. T. (2012). Landslide inventory maps: New tools for an old problem. *Earth-Science Reviews, 112*(1-2), 42-66.

Haneberg, W. C., Cole, W. F., & Kasali, G. (2009). High-resolution lidar-based landslide hazard mapping and modeling, UCSF Parnassus Campus, San Francisco, USA. *Bulletin of Engineering Geology and the Environment, 68*(2), 263-276.

Hede, A. N. H., Kashiwaya, K., Koike, K., & Sakurai, S. (2015). A new vegetation index for detecting vegetation anomalies due to mineral deposits with application to a tropical forest area. *Remote Sensing of Environment, 171*, 83-97.

Hung, L. Q., Van, N. T. H., Son, P. V., Ninh, N. H., Tam, N., & Huyen, N. T. (2017). *Landslide Inventory Mapping in the Fourteen Northern Provinces of Vietnam: Achievements and Difficulties*, Cham.

Jackson Jr, L., Bobrowsky, P., & Bichler, A. (2012). Identification, maps and mapping—Canadian technical guidelines and best practices related to landslides: A national initiative for loss reduction. *Geological survey of Canada, Open file, 7059*.

Kaur, H., Gupta, S., & Parkash, S. (2017). Comparative evaluation of various approaches for landslide hazard zoning: a critical review in Indian perspectives. *Spatial Information Research, 25*(3), 389-398.

Kocaman, S., Tavus, B., Nefeslioglu, H. A., Karakas, G., & Gokceoglu, C. (2020). Evaluation of floods and landslides triggered by a meteorological catastrophe (Ordu, Turkey, August 2018) using optical and radar data. *Geofluids, 2020*, 1-18.

Korup, O. (2005). Geomorphic imprint of landslides on alpine river systems, southwest New Zealand. *Earth Surface Processes and Landforms, 30*(7), 783-800.

Li, Z., Shi, W., Lu, P., Yan, L., Wang, Q., & Miao, Z. (2016). Landslide mapping from aerial photographs using change detection-based Markov random field. *Remote Sensing of Environment, 187*, 76-90.

Łuszczyńska, K., Wistuba, M., & Malik, I. (2017). Dendrochronology as a source of data for landslide activity maps–an example from Beskid Żywiecki Mountains (Western Carpathians, Poland). *Environmental & Socio-economic Studies, 5*(3), 40-46.

Marchesini, I., Santangelo, M., Fiorucci, F., Cardinali, M., Rossi, M., & Guzzetti, F. (2013). A GIS method for obtaining geologic bedding attitude. In *Landslide Science and Practice* (pp. 243-247): Springer.

Maxwell, A. E., Warner, T. A., & Guillén, L. A. (2021). Accuracy assessment in convolutional neural network-based deep learning remote sensing studies—part 1: Literature review. *Remote Sensing, 13*(13), 2450.

McKean, J., & Roering, J. (2004). Objective landslide detection and surface morphology mapping using high-resolution airborne laser altimetry. *Geomorphology, 57*(3-4), 331-351.

Mezaal, M. R., Pradhan, B., Sameen, M. I., Mohd Shafri, H. Z., & Yusoff, Z. M. (2017). Optimised neural architecture for automatic landslide detection from high-resolution airborne laser scanning data. *Applied Sciences, 7*(7), 730.

Mia, M., Sultana, N., & Paul, A. (2015). Studies on the causes, impacts and mitigation strategies of landslide in Chittagong city, Bangladesh. *Journal of Environmental Science and Natural Resources, 8*(2), 1-5.

Moosavi, V., Talebi, A., & Shirmohammadi, B. (2014). Producing a landslide inventory map using pixel-based and object-oriented approaches optimised by Taguchi method. *Geomorphology, 204*, 646-656.

Otukei, J. R., & Blaschke, T. (2010). Land cover change assessment using decision trees, support vector machines and maximum likelihood classification algorithms. *International Journal of Applied Earth Observation and Geoinformation, 12*, S27-S31.

Pawłuszek, K., Borkowski, A., & Tarolli, P. (2017). *Towards The Optimal Pixel Size of Dem for Automatic Mapping of Landslide Areas*. Paper presented at the International Archives of the Photogrammetry, Remote Sensing & Spatial Information Sciences.

Pirasteh, S., & Li, J. (2016). Landslides investigations from geoinformatics perspective: quality, challenges, and recommendations. *Geomatics, Natural Hazards and Risk, 8*(2), 448-465.

Razak, K. A., Bucksch, A., Damen, M., van Westen, C., Straatsma, M., & de Jong, S. (2013). Characterising tree growth anomaly induced by landslides using LiDAR. In *Landslide Science and Practice* (pp. 235-241): Springer.

Razak, K. A., Bucksch, A., Straatsma, M., Van Westen, C. J., Bakar, R. A., & De Jong, S. M. (2013). *High density airborne lidar estimation of disrupted trees induced by landslides.* Paper presented at the 2013 IEEE International Geoscience and Remote Sensing Symposium-IGARSS.

Santangelo, á., Cardinali, á., Rossi, á., Mondini, A., & Guzzetti, F. (2010). Remote landslide mapping using a laser rangefinder binocular and GPS. *Natural Hazards and Earth System Sciences, 10*(12), 2539-2546.

Santangelo, M., Marchesini, I., Bucci, F., Cardinali, M., Fiorucci, F., & Guzzetti, F. (2015). An approach to reduce mapping errors in the production of landslide inventory maps. *Natural Hazards and Earth System Sciences, 15*(9), 2111-2126.

Schuster, R. L. (1996). *Landslides: Investigation and Mitigation. Chapter 2-Socioeconomic Significance of Landslides*.

Schuster, R. L., & Highland, L. M. (2003). *Impact of landslides and innovative landslide-mitigation measures on the natural environment.* Paper presented at the International conference on slope engineering, Hong Kong, China.

Soeters, R., & Westen, C. J. (1996). *Slope instability recognition, analysis, and zonation*.

Tating, F. F. (2006). *Landslide Susceptibility Assessment Using Information Value Statistical Method: A Case Study On Northern Kota Kinabalu, Sabah.* Paper presented at the Proc. of International Symposium on Geotechnical Hazards: Prevention, Mitigation and Engineering Response, Yogyakarta, Indonesia.

Tien Bui, D., Shahabi, H., Shirzadi, A., Chapi, K., Alizadeh, M., Chen, W., . . . Hong, H. (2018). Landslide detection and susceptibility mapping by airsar data using support vector machine and index of entropy models in Cameron Highlands, Malaysia. *Remote Sensing, 10*(10), 1527.

Van Westen, C. J., Van Asch, T. W. J., & Soeters, R. (2006). Landslide hazard and risk zonation—why is it still so difficult? *Bulletin of Engineering Geology and the Environment, 65*, 167–184. doi:https://doi.org/10.1007/s10064-005-0023-0

Wang, D., Hollaus, M., Puttonen, E., & Pfeifer, N. (2016). Automatic and self-adaptive stem reconstruction in landslide-affected forests. *Remote Sensing, 8*(12), 974.

Wang, D., Hollaus, M., Schmaltz, E., Wieser, M., Reifeltshammer, D., & Pfeifer, N. (2016). Tree stem shapes derived from TLS data as an indicator for shallow landslides. *Procedia Earth and Planetary Science, 16*, 185-194.

Wistuba, M., Malik, I., Gärtner, H., Kojs, P., & Owczarek, P. (2013). Application of eccentric growth of trees as a tool for landslide analyses: The example of Picea abies Karst. In the Carpathian and Sudeten Mountains (Central Europe). *Catena, 111*, 41-55.

Yan, L., Gong, Q., Wang, F., Chen, L., Li, D., & Yin, K. (2023). Integrated Methodology for Potential Landslide Identification in Highly Vegetation-Covered Areas. *Remote Sensing, 15*(6), 1518.

Yang, W., Qi, W., Wang, M., Zhang, J., & Zhang, Y. (2017). Spatial and temporal analyses of post-seismic landslide changes near the epicentre of the Wenchuan earthquake. *Geomorphology, 276*, 8-15.

Zhang, L., Huang, R., Pei, X., & Li, S. (2016). Evolution analysis of a toppling landslide based on trees' growing—A case study of Erguxi Landslide, Lixian county, China. In *Landslides and Engineered Slopes. Experience, Theory and Practice* (pp. 2107-2112): CRC Press.